ELSEVIER

Journal of Structural Geology 26 (2004) 2119–2137

JOURNAL OF STRUCTURAL GEOLOGY

www.elsevier.com/locate/jsg

Detachment folding in the Southwestern Tian Shan–Tarim foreland, China: shortening estimates and rates

K.M. Scharer[a,*], D.W. Burbank[b], J. Chen[c], R.J. Weldon[a], C. Rubin[d], R. Zhao[c], J. Shen[c]

[a]*Department of Geological Sciences, 1272 University of Oregon, Eugene, OR 97403, USA*
[b]*Department of Geological Sciences, University of California, Santa Barbara, CA 93106, USA*
[c]*State Key Laboratory of Earthquake Dynamics, Institute of Geology, China Seismological Bureau, P.O. Box 9803, Beijing 100029, P.R. China*
[d]*Department of Geological Sciences, Central Washington University, Ellensburg, WA 98926, USA*

Received 17 February 2003; received in revised form 15 January 2004; accepted 26 February 2004

Available online 20 July 2004

Abstract

Geologic observations of the Chinese Tian Shan foreland reveal active, contractional deformation along the entire margin. To quantify the amount of shortening and understand the structural style, we mapped the stratigraphy and structure of four folds expressed at the western end of the foreland, north of Kashi. In this region, upper Tertiary through Quaternary sediments are conformable, but an abrupt transition from parallel to unconformable bedding in the uppermost strata suggests a transition from pre-fold strata to strata deposited on a growing fold. The folds have very steep (60–90°) limbs and are box-like to isoclinal, suggestive of detachment folding. Total north–south shortening across the center of the region is >9 km, of which 5–7 km occurred in the Kashi–Atushi fold system. Shortening estimates determined with excess area methods for individual folds decrease from a maximum of 6.8 km in the northwest to a minimum of 0.7 km in the southeast. Timing derived from a paleomagnetic study shows that the transition to syn-folding strata occurred ~1.2 Ma in the middle of the study area, resulting in an average shortening rate for the Kashi–Atushi fold system of ~5 mm/yr if folding was coeval. The shortening rate is high compared with foreland deformation east of the study area, suggesting that the regional stresses or response of the foreland stratigraphy are unique to the Kashi–Atushi fold system kinematics.

Keywords: Kashi Depression; Xiyu conglomerate; Lateral propagation; Growth strata; Anticline; Kepingtage

1. Introduction

The Tian Shan (Fig. 1) have been the focus of recent geologic investigations concerning the timing, sequence, and geometry of active, intracontinental mountain building (Sobel and Dumitru, 1997; Yin et al., 1998; Allen et al., 1999; Burchfiel et al., 1999; Sobel et al., 2000; Abdrakhmatov et al., 2002; Thompson et al., 2002). These studies suggest that the onset of deformation in the Tian Shan began about 20 Ma, or ~35 Myr after the initial Indo-Asian collision, and that north–south directed shortening continues to be active across the entire range. Thompson et al. (2002) demonstrate that at late Pleistocene time scales, ~13 mm/yr of shortening is accommodated on 5–6 discrete structures distributed across the Kyrgyz Tian Shan. Geodetic studies indicate that up to 50%, or 20–24 mm/yr, of the total modern convergence between the Indian and Eurasian plates is accommodated by shortening in the Tian Shan (Abdrakhmatov et al., 1996; Holt et al., 2000; Wang et al., 2000). The geologic and geodetic observations agree well in the Kyrgyz Tian Shan, which suggests that the remaining, geodetically calculated shortening of ~7–10 mm/yr should occur south of the Aksay Basin in the southern Tian Shan and northern Tarim Basin (Fig. 1).

Studies in the central and eastern Tian Shan foreland have estimated the Cenozoic shortening, but provided loose control on the timing of the deformation in the western foreland (Yin et al., 1998; Allen et al., 1999; Burchfiel et al., 1999). In the southwestern Chinese Tian Shan foreland, up to 12 km of Cenozoic strata (Bally et al., 1986) provide a pristine succession in which the style, age, and rates of shortening can be investigated. This paper presents structural, stratigraphic and geomorphic data to define the style of folding in this region. In combination with a

* Corresponding author. Tel.: +1-514-346-4573; fax: +1-514-346-4692.
E-mail address: kscharer@darkwing.uoregon.edu (K.M. Scharer).

0191-8141/$ - see front matter © 2004 Elsevier Ltd. All rights reserved.
doi:10.1016/j.jsg.2004.02.016

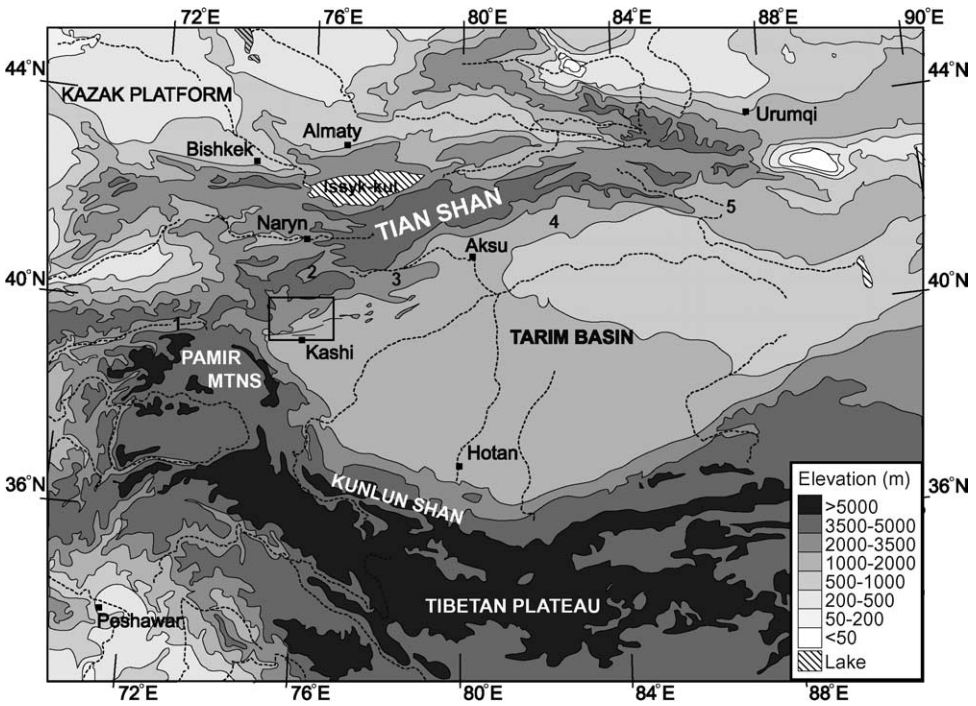

Fig. 1. Elevation map of the Tarim Basin, Tian Shan, Pamir Mountains, and Northern Tibetan Plateau. Major rivers designated with dashed lines, lake (Issyk-kul) in stripes. The study area is located in the western corner of the Tarim Basin, surrounded to the north, west, and south by >4000 m peaks. The box north of Kashi locates Fig. 2. Number 1 locates the Alai Valley and 2 locates the Aksay Valley described by Thompson et al. (2002). Numbers 3–5 locate the Kepingtage, Kuche, and Boston Tokar/Kalasu River sections of Allen et al. (1999), Yin et al. (1998), and Burchfiel et al. (1999), respectively.

magnetostratigraphic study presented by Chen et al. (2002), we estimate the timing of initiation of folding and quantify regional shortening rates. We show that structures in the northwest Tarim Basin are detachment folds that began deforming during the Pleistocene and have accommodated much of the recent shortening predicted geodetically to occur south of southern Kyrgyzstan.

1.1. Geographic and geologic setting

The Tian Shan extends over 2000 km eastward from Tajikistan, covers most of Kyrgyzstan, and tapers to the east in the Xinjiang province of western China At the study location, the range is ~500 km wide. The Tarim Basin is an internally draining, trapezoid shaped basin 1500 km long, pinched between the Tian Shan on the north, the Pamir Mountains to the west, and the Tibetan Plateau to the south. The field area is located in the northwest corner of the Tarim Basin, approximately 250 km from the Alai Valley where the Tian Shan and the Pamir Mountains meet (Fig. 1). The arid climate and the paucity of vegetation provide excellent exposure for structural and stratigraphic mapping.

The Tian Shan and the Tarim Basin blocks have been proximate since the Devonian, when an intervening ocean basin separating the two began subducting under the ancestral Tian Shan (Watson et al., 1987; Carroll et al., 1995). The two blocks were sutured by the late Permian (Carroll et al., 1995; Yin and Nie, 1996) and have subsequently felt the effects of at least three Mesozoic collisions south of the Tarim craton (Hendrix et al., 1992). The period between the last Mesozoic collision, when the Kohistan–Dras arc–forearc complex was accreted to southern Asia (~70 Ma), and the initiation of Cenozoic deformation in the Tian Shan (~25 Ma) was a time of tectonic quiescence. During this ~45 Myr period, the ancestral Tian Shan was beveled by erosion. Stratigraphically, this period is represented by a widespread, planar denudation surface in the Tian Shan (Abdrakhmatov et al., 2002) and by deposition of lower Tertiary strata along its margins (Bally et al., 1986; Hu, 1992). Within the Tian Shan proper, the Cenozoic deformation has been quantified by studying the uplift and faulting of the early Tertiary peneplain (Burbank et al., 1999; Bullen et al., 2001; Abdrakhmatov et al., 2002; Thompson et al., 2002). At the southern margin of the Tian Shan, the peneplain is absent, but deformation of foreland fold-and-thrust sequences has been used to understand the timing and style of the outward growth and uplift of the Tian Shan (Sobel and Dumitru, 1997; Yin et al., 1998; Allen et al., 1999; Burchfiel et al., 1999; Chen et al., 2001, 2002).

Geophysical evidence, numerical modeling, and both geologic and geomorphic evidence suggest that the Tarim Basin is being coherently thrust under the Tian Shan (Molnar and Tapponnier, 1975; Burov et al., 1990; Avouac et al., 1993; Burtman and Molnar, 1993; Neil and House-

man, 1997; Burchfiel et al., 1999; Abdrakhmatov et al., 2002). Sediments express the convergence in a series of folds and thrust faults along the northern margin of the Tarim Basin (Rubin et al., 2000; Scharer et al., 2000; Zhao et al., 2000; Chen et al., 2001). The topographic front of the Tian Shan proper is delineated by the South Tian Shan fault, an oblique reverse fault with unknown displacement magnitude (Yin et al., 1998). Basinward of the South Tian Shan fault, two areas with contrasting deformational styles are clear in Landsat Multispectral Scanner imagery (Fig. 2). The northern area, called the Kepintage–Yishilakekalawuer thrust fault (Kepingtage), represents the westernmost expression of the Kashi–Akesu system as identified by Yin et al. (1998). It is characterized by south verging thrust faults that place Paleozoic strata on top of Mesozoic and Cenozoic sediments (XBGM, 1985; Sobel and Dumitru, 1997; Rubin et al., 2000; Zhao et al., 2000; Chen et al., 2001, 2002). Fission track dating by Sobel and Dumitru (1997) suggests that deformation propagated southward from the Tian Shan, exhuming this part of the Kepingtage system since ~14 Ma. Total shortening in this part of the Kepingtage has not been calculated, but folded sediments in piggyback basins provide evidence for a component of late Tertiary deformation.

The southern area, the Kashi–Atushi fold system, is south of the Kepingtage system. It includes the towns of Kashi (Kashgar) and Atushi (Artush), and is characterized by two rows of sinuous folds within the Kashi Depression, a deep Tertiary sub-basin. Major rivers draining the Tian Shan cross the Kashi–Atushi fold system. Large earthquakes have occurred at the perimeter of this area, but none are recorded within the fold system (Fig. 3). We differentiate this area from the Kashi–Akesu system of Yin et al. (1998) due to the striking difference between the

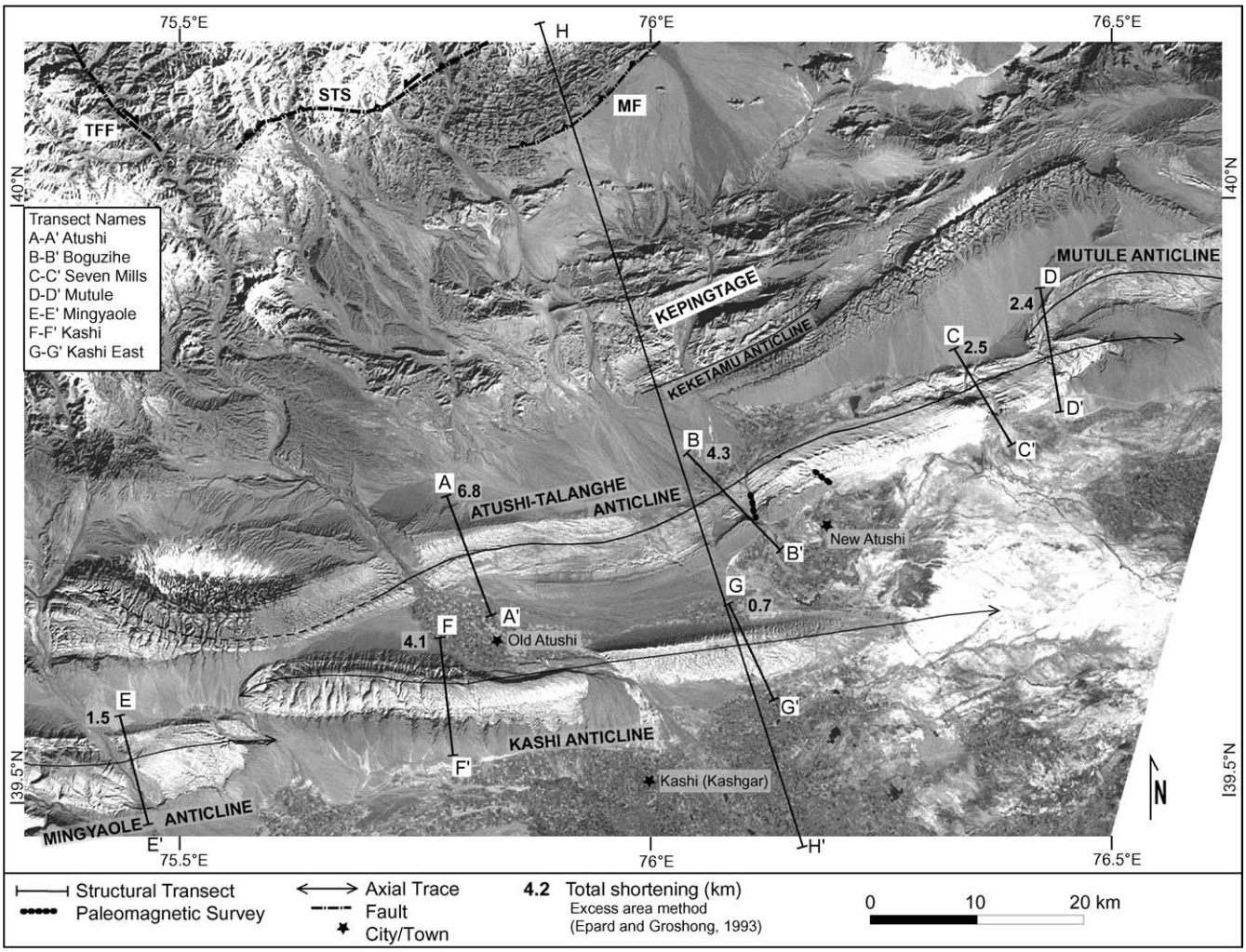

Fig. 2. Landsat image of the southwestern Tian Shan. The study area is located south of the Southern Tian Shan fault (STS), the Muziduke fault (MF), and the Kepingtage–Yishilakekalawuer Thrust Fault system (Kepingtage). The timing and displacements of these faults are poorly constrained. TFF is the Talas–Ferghana fault, a right lateral fault with ~10 mm/yr Cenozoic slip rate (Burtman et al., 1996). The Kashi–Atushi fold system covers the lower half of the image. Upper Tertiary strata (light color) comprise most of the folds, which are rimmed by resistant Quaternary conglomerates (dark color distinct on the southern limbs). The Talas–Ferghana fault projects into the middle of the fold system, which appears unaffected, suggesting right-lateral strain on the Talas–Ferghana fault is partitioned into the South Tian Shan fault or the Muziduke fault rather than the Tarim craton.

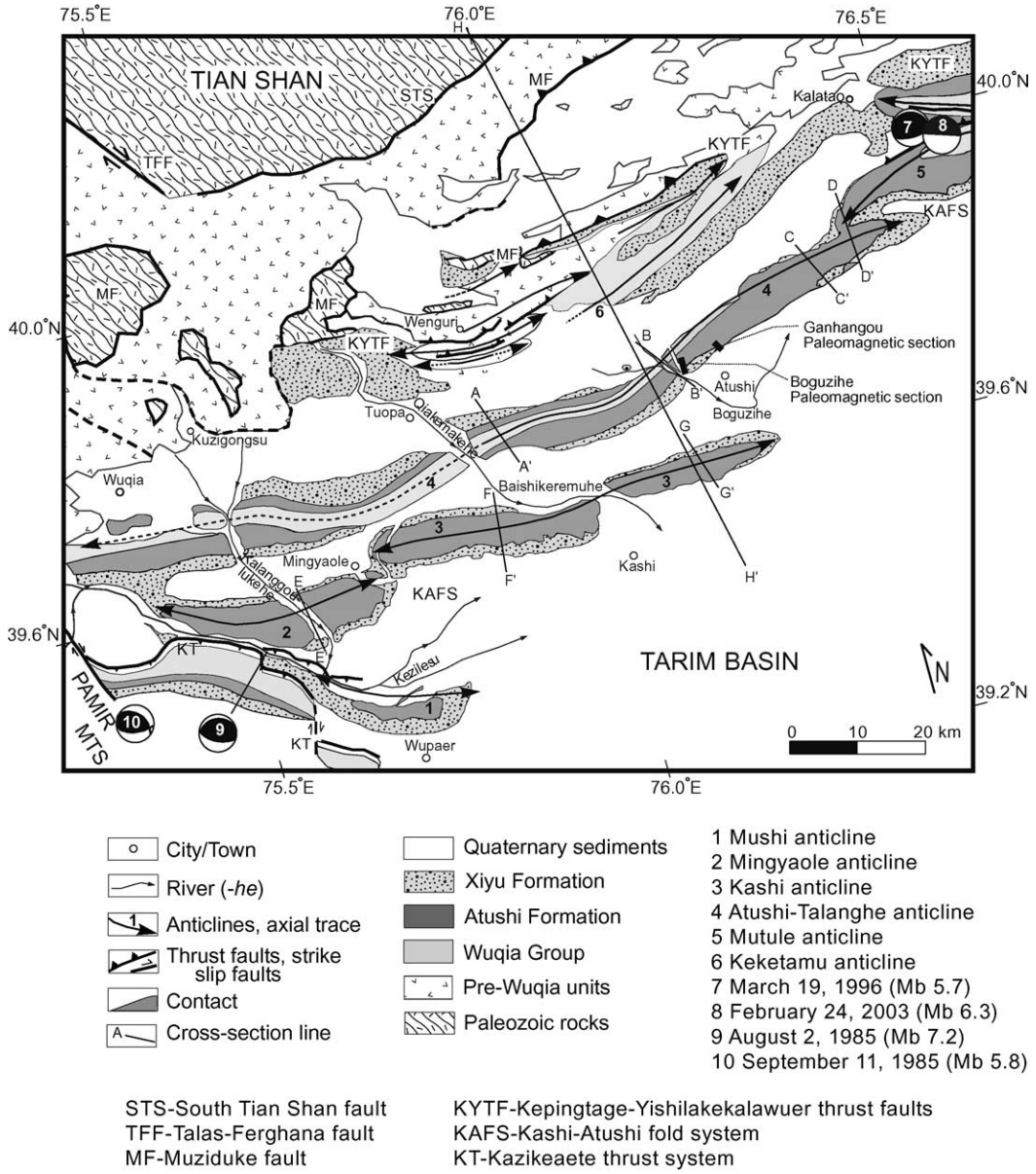

Fig. 3. Geologic map of Kashi–Atushi fold system, modified from Chen et al. (2002). Note that the Xiyu Formation pinches out along strike and is located closer to the axial trace on the north side of each anticline. The Boguzihe ('he' means river in Chinese) has eroded the northern limb of the eastern end of the Atushi–Talanghe anticline. Focal mechanisms (Harvard CMT, 2003) of major earthquakes show north-directed, low angle reverse faulting; the 1902 ~M 7.7 Artux earthquake is located just east of the map area (Molnar and Ghose, 2000).

imbricate thrust stacks of Mesozoic and Paleozoic strata that form the northern band of deformation in the Tarim Basin and the simply folded upper Cenozoic strata in the study area. The Kashi–Atushi fold system includes the Atushi–Talanghe, Mutule, Mingyaole and Kashi anticlines. We present fieldwork from the summers of 1999, 2000, and 2003, which includes six structural transects across the folds (Fig. 2). We incorporate the magnetostratigraphic dating on the Atushi–Talanghe anticline presented by Chen et al. (2002) to constrain the timing and rates of this shortening. The discussion evaluates the mechanisms of detachment folding and the regional setting that produced this unique deformation.

2. Stratigraphy

Although not exposed in the study area, we review the lithology and interpreted depositional setting of the pre-Tertiary sediments because they are involved in, and to some extent may control, the modern deformation and structural behavior of the system. As a depocenter, the field area shares many attributes with the Southwest Depression that borders the Kunlun Shan (Fig. 1; Hu, 1982; Sobel and Dumitru, 1997). The Paleozoic rocks across the western Tarim Basin comprise ~4000 m of neritic carbonates and shallow marine carbonates interbedded with mudstone and shale, recording a series of marine transgressions and

regressions. No Triassic sediments are reported in the Kashi region, whereas Jurassic coal bearing sediments range in thickness from 1400 to 3800 m. Lower Cretaceous mudstone and sandstone approximately 1000 m thick was deposited before an eastward transgression of the Tethys Sea occurred in the late Cretaceous (Hu, 1982; Sobel, 1999).

Isopachs depict Tertiary through modern clastic sediments exceeding 10,000 m in the Kashi Depression (Bally et al., 1986); in a different study a lower value of ~8000 m is cited (Hu, 1992). These strata are subdivided into the Paleogene Kashi Group, the Neogene Wuqia Group and the Atushi and Xiyu Formations (Fig. 4; Hu, 1982; Mao and Norris, 1988). The Paleogene Kashi Group records a series of alternating shallow marine, hypersaline lagoon, and fluvial deposits. The thickest members of the Kashi Group include the 200-m-thick massive gypsum and limestone of the Aertashi Formation, the red, purple and gray–green mudstone and siltstone of the Bashibulake Formation (>268 m) and the Oligocene Kezilouyi Formation, a brown mudstone and gray–green sandstone with numerous gypsum interbeds (>280 m; Mao and Norris, 1988; Yang, 1996). The Kashi Group is exposed in the southern edge of the Kepingtage system (Fig. 3).

Neogene through modern strata are exposed by the Kashi–Atushi fold system (Fig. 3; Zhou and Chen, 1990; Chen et al., 2001, 2002). Red mudstone exposed in the core of the Atushi fold is inferred to correlate with the multicolored Wuqia Group, dated elsewhere by faunal assemblage as late Oligocene through Miocene (Hu, 1982). Conformably above the Wuqia Group, the Atushi Formation is dominated by yellow–gray to tan mudstone, siltstone, and fine- to medium-grained sandstone. Thin beds, 5–50 mm thick, of gypsum and gypsiferous mudstone are preserved within the lower section; higher the section contains rare small pebble conglomerate layers. In the field area, paleocurrent directions in the upper Tertiary clastics are oriented predominantly southeast.

The top of the Atushi Formation is marked by an abrupt coarsening and darkening of the lithology that is easily mapped in the study area and indicates transition into the Xiyu Formation (Fig. 5). At the base of the Xiyu Formation, 0.3–7-m-thick pebble conglomerate beds alternate with poorly sorted sand lenses and discontinuous silt and sand layers with scarce pebbles. Higher in the section, the conglomerate beds are thicker and comprised of well rounded, clast supported pebbles and cobbles; less common are beds with thicknesses of 5–15 m, which are matrix supported. The Xiyu Formation varies from 0 to 2500 m thick. Clast composition of the Xiyu Formation is dominated by limestone and sandstone clasts derived from Paleozoic to Mesozoic strata in the Kepingtage system and the southern Tian Shan, and is similar to the modern, southeast flowing rivers in the study area.

The Xiyu and Atushi Formations appear conformable, but the stratigraphic level of the contact varies along strike. The character of the contact can be seen in the Landsat imagery (Fig. 2) where, for example, west of transect line F–F′ the contact creeps down section or east of the B–B′ traverse on the Atushi–Talanghe anticline, the dark Xiyu Formation conglomerate tapers out within the lighter Atushi sediments. These along-strike variations suggest interdigitation of different depositional systems during systems during the late Cenozoic.

2.1. Progradation

The stratigraphic height of the Atushi–Xiyu contact also appears to vary in a north–south direction, but consistently

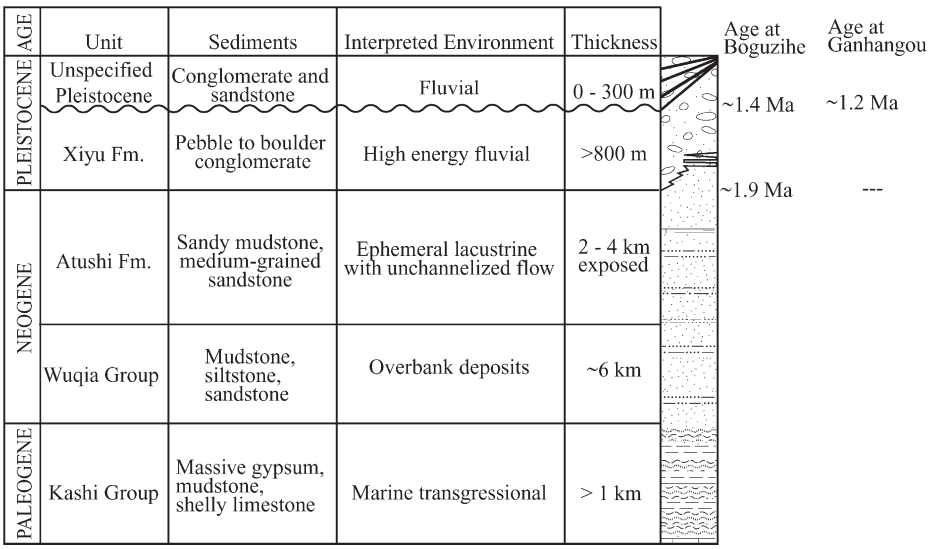

Fig. 4. Cenozoic stratigraphy exposed by folding includes over 5 km of Neogene through mid-Pleistocene fine-grained sediments capped by lower to middle Pleistocene conglomerates. The Kashi Group is exposed along parts of the southern edge of the Kepingtage. The combined thickness of the Tertiary sediments is ~10 km in this region (Bally et al., 1986). According to Sobel (1999) and Chinese geological maps, the oldest exposed sediments are Miocene (XBGM, 1965a,b). Pleistocene ages presented in Chen et al. (2002).

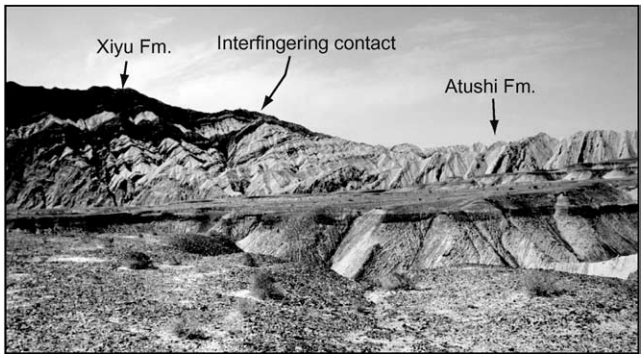

Fig. 5. Time-transgressive nature of major lithostratigraphic boundaries illustrated by interfingering Atushi and Xiyu Formations at the Boguzihe water gap. View is to the SSW, across a terrace of the Boguzihe on the southern limb of the Talanghe anticline. Hill at left is ~250 m high.

across the region. This variation is shown in the distance between the axial surface and the Xiyu Formation on the north versus the south flank of each fold (Figs. 2 and 3). Despite the essentially identical geometry of the fold limbs and an absence of major thrust faults, the Atushi–Xiyu contact on the north side of each fold is consistently 1.5–2 times closer to the core than the contact is on the south side. Along the Atushi–Talanghe anticline, the contact on the northern limb is ~1.5 km lower stratigraphically than on the southern limb. The difference is reduced to ~0.5 km across the more southerly Mingyaole and Kashi anticlines. This spatial variation in the thickness of the Xiyu Formation demands explanation because the conglomerate unit offers the only potential stratigraphic control with which to produce cross-sections across the folds (the gradual color change between the Wuqia Group and Atushi Formation makes this older contact ambiguous). Two mechanisms, structural or stratigraphic, could account for the spatial variation.

A structural model suggests that beds on the northern limbs have been thinned during folding (Fig. 6A). The structural model predicts that the Xiyu Formation would be thinned on the northern side and that the axial traces would not bisect the neighboring kink panels. Poor preservation and/or exposure of the conglomerate on the northern side of the folds make these observations difficult, so we consider variation in mesoscopic deformation across the fold. The shear needed to thin the northern limb by ~1.5 km should require significant penetrative shear across the bedding. Shear strains of ~15% can be observed in mesoscopic studies around fault zones (Jamison, 1989), suggesting that thinning the forelimb by 50% should create obvious shear and deformation within the attenuated limb. During structural mapping, we observed no significant difference in mesoscopic deformation between the limbs. On the contrary, bedding planes were well maintained in each limb even where wide panels of the limb were steeply dipping or overturned.

The stratigraphic model relies on a wedge shaped upper unit (in cross-section) to cause the difference in the

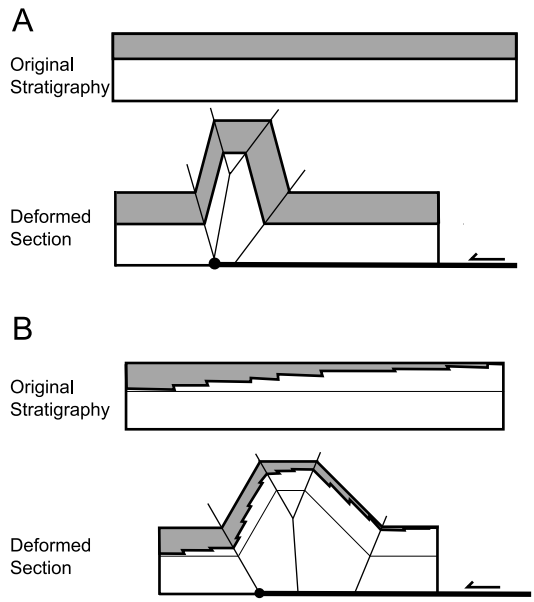

Fig. 6. Models to account for map trace of Xiyu Formation. (A) Shear during folding thins units in the forelimb. In this model, the base of the gray unit in the forelimb is ~2.5 times closer to the fold axis than the base of the gray unit on the backlimb. (B) When folded, a progradational contact will be farthest from the axial surface on the distal side (assuming no limb thinning). In this cartoon, the backlimb contact is twice as far from the core as the forelimb contact.

stratigraphic thickness across the fold (Fig. 6B). Given both the observed variations in the thickness of the contact and absence of penetrative shear preferential to either limb, we interpret that the Xiyu Formation is wedge shaped. Furthermore, the contact appears to be conformable. A conformable, wedge shaped unit in this setting can be created by progradation into a subsiding foreland basin. If the unit is a progradational wedge, the contact should be older at the northern limb and younger at the southern limb. Given these stratigraphic and structural considerations, we interpret the contact to be progradational and relatively younger on the southern limb than on the northern limb of each fold. A similar appearing conglomerate, commonly called the Xiyu Formation, is widespread across the Tian Shan foreland and, without quantitative constraints, has been interpreted to correlate with a ~2.5 Ma climate change (Avouac et al., 1993; Burchfiel et al., 1999; Zhang et al., 2001). Our interpretation at the Kashi–Atushi fold system indicates, however, that the base of the conglomerate is temporally variable, ranging from 2.8 to 1.9 Ma across the Talanghe anticline (Chen et al., 2002).

2.2. Growth strata

Bedding is conformable within the folds but not at the southernmost exposed flanks at each of the transects across the Atushi–Talanghe and Kashi anticlines At these transects, field observations show that in the last hundreds of meters of exposed strata, the bedding inclinations decrease abruptly up section, and in most places form

angular unconformities suggestive of off lapping. The Ganhangou paleomagnetic section was located to capture this transition (Fig. 7). In contrast, mapping at the Mingyaole anticline revealed that a few closely spaced unconformities are located just below the base of the Xiyu Formation. A transition from conformable beds to off lapping or angular unconformities is frequently interpreted to result from the transition from static conditions to active folding (e.g. Poblet et al., 1997). We argue that the gently dipping outer beds are syntectonic strata, deposited after the initiation of folding in the region.

At the Seven Mills and Atushi transects, the southern flanks show continuous reduction in dips of off lapping strata; however, the northern flanks revealed dramatic changes in dip. At the Atushi transect, for example, a wide, 75° north dipping panel is overlain by a 15° dipping panel. We infer that, as observed today, rivers eroded the north side of the folds as they grew, and that growth strata were not preserved until later in the development of the fold, when these sections had risen above the grade of the river. It appears that the southern sides of the folds were sheltered from this effect, and growth strata were deposited continuously.

3. Structure

We conducted detailed field mapping on six traverses across the Atushi–Talanghe, Mutule, Mingyaole and Kashi anticlines to investigate the variation in shortening and deformational style across the Kashi–Atushi fold system (Fig. 2). Transects were located along water gaps or roads cutting orthogonal to the structures to maximize access to structures and bedding exposures. Structural and sedimentological data were mapped at ~1:25,000 onto CORONA satellite photographs, aerial photos, and topographic maps. Additional structural data were interpreted from Chinese geologic maps (XBGM, 1965a,b). Field maps were later transferred onto a geographic information system database with the Landsat image and CORONA photographs tied to a 90 m digital elevation model (DEM) base. Topographic profiles oriented perpendicular to the average strike of the bedding orientation at each traverse were derived from the DEM and used as bases for our cross-section interpretations.

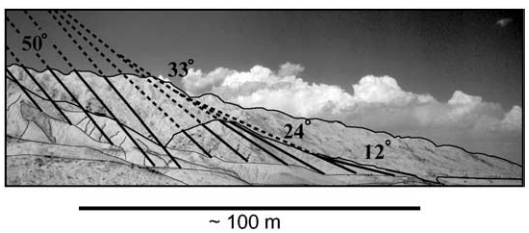

Fig. 7. Interpreted photograph of growth strata on the southern limb of the Talanghe anticline at the Ganhangou paleomagnetic transect. View is to the east. South of a ~3-km-wide panel dipping 50°, off lapping dips of siltstone and small-pebble conglomerates (foreground) are interpreted to record the initiation of folding. Pale hill under skyline is the eastward continuation of Talanghe anticline.

The cross-sections are constrained by structural measurements, stratigraphic thickness based on field measurements, progradation of the conglomerate unit, and unpublished seismic data. Our interpretations suggest most of the folds would reach 3–4 km above the land surface, yet modern topography exhibits less than 1 km of relief (Figs. 8 and 9). Due to the vigorous erosion and lack of distinctive stratigraphic marker beds, two techniques were used to quantify the amount of shortening across the region. We review the general method for creating the cross-sections, summarize general observations from the seismic reflection data, discuss the common structural style of the folds, and then report details of each fold individually.

The basic fold geometry was determined by fitting a form line to the structural data. Where canyon walls reveal cross-sectional views, the Kashi–Atushi fold system exhibits sharp kink axes in the limbs, while sheared zones were common in the core of tight folds. These features are well-modeled using kink style fold axes to separate dip panels (Marshak and Mitra, 1988). Dip panel width and inclination were determined by converting dip measurements into apparent dip with respect to the cross-section trend, grouping the dip measurements into internally consistent sets (variability $\leq 15°$) and calculating the average angle (Figs. 8 and 9). Where we were able to measure bedding thicknesses across a kink axis, the thicknesses did not change, indicating that the kink axes bisects the kink panels. In each cross-section, the stratigraphic height of the growth strata within each fold limb is accurate, but the geometry of the growth strata package is idealized. For simplicity (and lacking evidence to the contrary), we assumed that there is no change in structural height from north to south across the structures.

3.1. Seismic reflection data

We examined three unpublished, confidential seismic reflection images from transects across the Atushi–Talanghe and Kashi anticlines The seismic profiles are basically co-located with three traverses (Fig. 3): (1) over the Atushi–Talanghe anticline along the road at A–A′ and continuing through the Kashi anticline along the Baishikeremu River, (2) over the Atushi–Talanghe anticline at B–B′ and crossing the eastern edge of the topographic expression of the Kashi anticline, and (3) over the Atushi–Talanghe anticline at C–C′ and continuing ~20 km into the evaporite deposits ~15 km east of the end of the topographic expression of the Kashi anticline. These profiles fortuitously provide this study with a second perspective for interpreting the structures at depth.

The most valuable information in the seismic lines was the presence of long, gently dipping (~12°) reflectors at the outermost flanks of the folds, where young alluvial deposits on the surface prohibited access to the structure. The gently

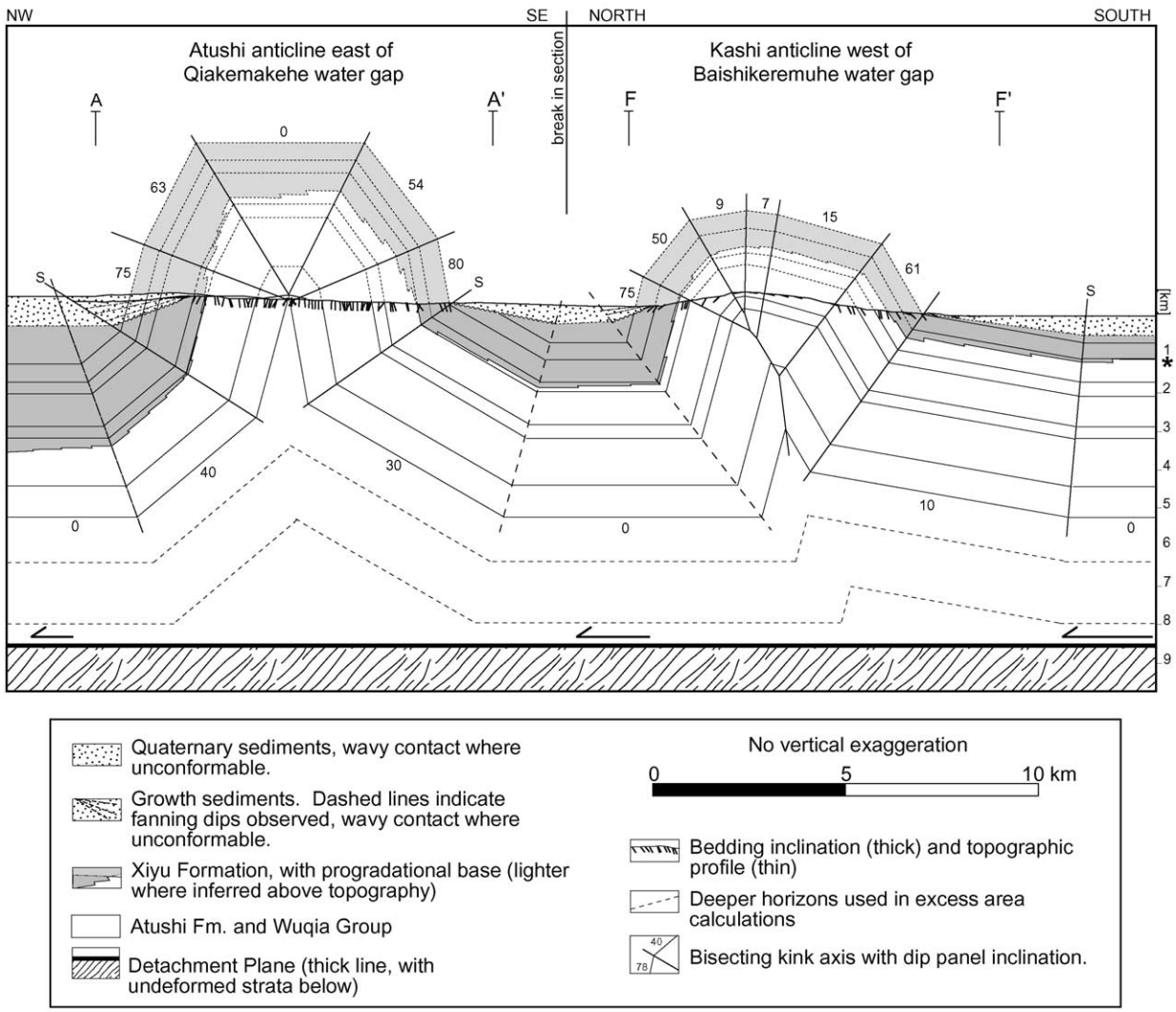

Fig. 8. Combined cross-section of Atushi and central Kashi transects. The depth to the detachment surface is determined from excess area calculations; the widths of the structures are constrained by surface exposures and the outer limit of folding expressed in the seismic images. Deeper horizons are dashed because they are used in area calculations; we do not prescribe the actual deformation style at these levels. Detachment folding occurs either due to an abrupt decrease in the magnitude of slip across the structure or a horizontal fault tip where displacement stops. Fanning dips at the outer edges of the folds are interpreted to represent growth strata. Where observed in the field the fanning dips are drawn on the image, otherwise the Quaternary sediments are unmarked. 'S' indicates approximate location of kink axis determined from seismic reflection profile. Dip of kink panels with no structural data is determined from seismic data (if bordered by kink axis labeled with an S) or results from the constraint that there is zero structural height developed across a fold (dashed). The asterisk ($*$) identifies the bed used to calculate line length shortening.

dipping outer limbs bracketed regions of discontinuous and unresolved reflectors positioned directly below the topographic expression of the folds, and correlate with measured bedding dips greater than $\sim 45°$. In the cross-section interpretations (Figs. 8 and 9), the gently dipping flanks seen in the seismic surveys are included, resulting in anticlines that are wider than evidenced in the topography.

Another common feature in each of these profiles is an essentially flat lying, strong reflector at 9–10 km below land surface, with the exception of Seven Mills, which was 12 km below land surface. From 5 km below land surface to the strong reflector at ~ 9 km, the reflectors are gently warped or discontinuous. Stratigraphically, 9–10 km is the approximate depth of a massive gypsum unit of the Aertashi Formation and other gypsiferous units within the Kashi Group (Yang, 1996). The variation in deformation with depth indicates several horizons may have accommodated different amounts of strain in this convergent setting.

3.2. Field observations and structural model

At the surface, most of the folds exhibit steep limbs dominated by dip panels inclined between 60 and 85° (overturned) The similarity between the largest, steepest, dip panel on each side of a fold obscures vergence, but in general, a subtle north vergence of the folds is exhibited in the cross-sections. The fold cores are tight, resulting in box-like to isoclinal knobs that rise off the low angle flanks (Figs.

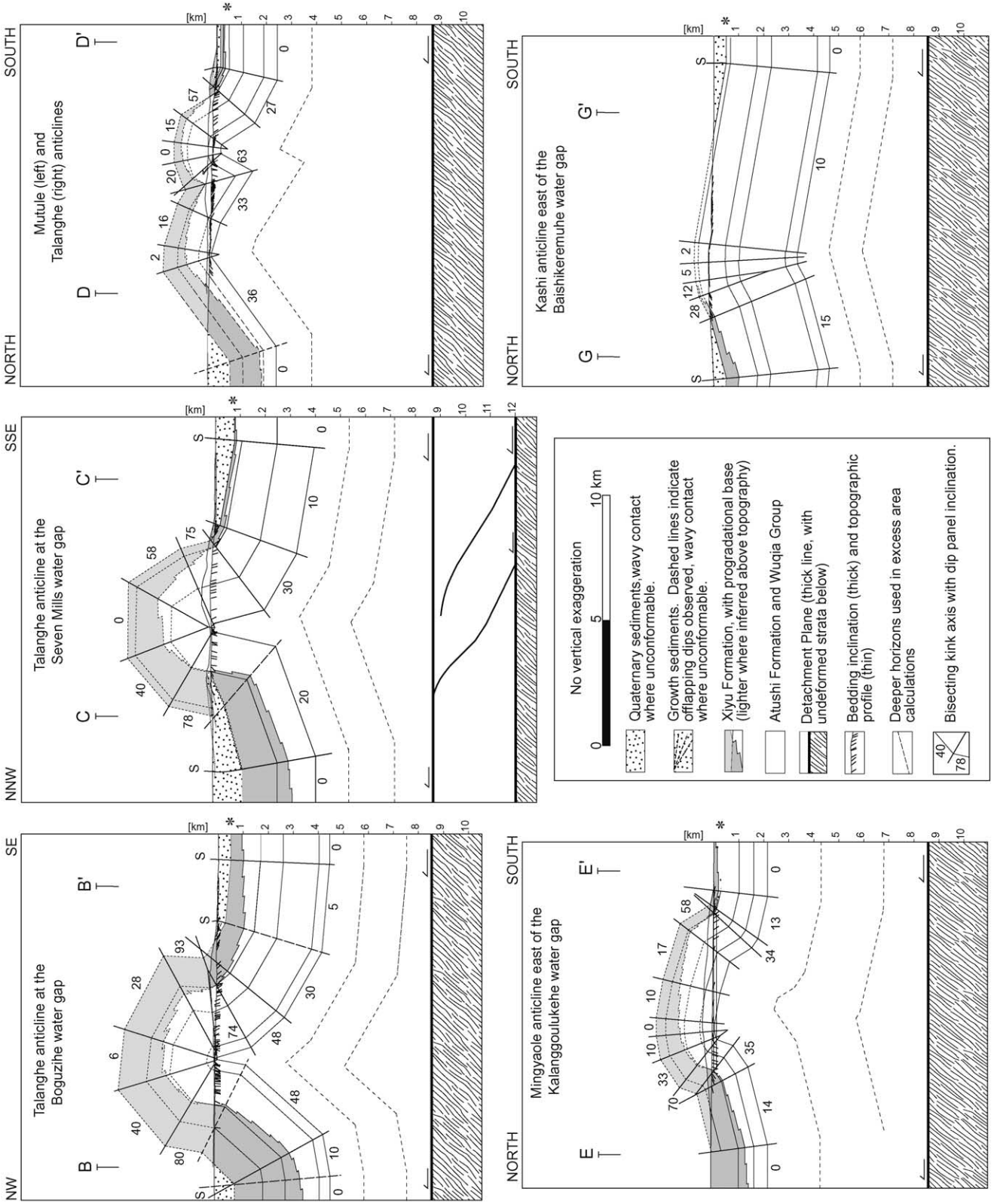
NW
SE
Talanghe anticline at the Boguzlhe water gap
B
B'
NNW
SSE
Talanghe anticline at the Seven Mills water gap
C
C'
NORTH
SOUTH
Mutule (left) and Talanghe (right) anticlines
D
D'
NORTH
SOUTH
Kashi anticline east of the Baishikeremuhe water gap
G
G'
NORTH
SOUTH
Mingyaole anticline east of the Kalanggoulukehe water gap
E
E'
[km]
No vertical exaggeration
0
5
10 km
Quaternary sediments,wavy contact where unconformable.
Growth sediments. Dashed lines indicate offlapping dips observed, wavy contact where unconformable.
Xiyu Formation, with progradational base (lighter where inferred above topography)
Atushi Formation and Wuqia Group
Detachment Plane (thick line, with undeformed strata below)
Bedding inclination (thick) and topographic profile (thin)
Deeper horizons used in excess area calculations
Bisecting kink axis with dip panel inclination.
40
78

8 and 9). To accommodate the steep bedding dips of the inner panels, the folds can be modeled as fault propagation folds with complex, imbricate blind faulting histories (Al Saffar, 1993) or as detachment folds. Basic observations suggest the anticlines are not fault propagation folds. (1) There is no evidence for long thrust ramps above 6 km below land surface in the seismic images. (2) Along some transects, fault scarps were observed near the core of the folds, but never at the base of the forelimb where a thrust fault is predicted from traditional fault propagation fold geometry (e.g. Suppe and Medwedeff, 1990). Instead, the geometry of the anticlines is consistent with models of disharmonic detachment folds (Mitra and Namson, 1989) or faulted detachment folds with moderate strain (Figure 3b in Mitra, 2002). Common to both of these models is a contrast between relatively competent layers deforming primarily by flexural slip that overlie incompetent units deforming by distributed or inhomogeneous deformation. The stratigraphic units at the Kashi–Atushi fold system exhibit a similar pattern, best observed at the Boguzihe profile (B–B′, Fig. 3). At the hinge zone of the fold, the lowest river terrace risers reveal that Wuqia Group bedding is obliterated, showing discontinuous blocks of bedded strata floating and chaotically rotated within a sheared mudstone matrix. Above this, the older river terrace risers reveal the Atushi Formation bending unbroken across the axial trace.

The cross-sections (Figs. 8 and 9) were constructed as detachment folds, constrained by structural measurements and the low dip panels observed in the seismic sections. Specific information on each profile is presented in the sections below. Each cross-section interpretation was drawn reducibly, meaning that axial planes were located to minimize the length of steeply dipping panels and maximize gently dipping panels. Short sections of moderate to gently dipping beds on the crest of the fold were included, resulting in rounded folds with minimized shortening.

3.2.1. Atushi–Talanghe anticline

The topographic expression of the Atushi–Talanghe anticline extends eastward over 100 km from the margin of the Pamir Mountains. Constrained by our structural transects and a strike line trace, the axial trace curves up to the northeast in several gentle arcs, lost finally to a series of deflected channels that drain southward from the Mutule anticline (Fig. 2). The fold is oriented approximately N72E. Previous mapping (Scharer et al., 2000) separated the western, Atushi fold from the eastern Talanghe fold at an eastward plunging core visible to the east of the Atushi transect line (A–A′) in Fig. 2. However, subsequent structural mapping along the southern limb east transect A–A′ (Fig. 8) showed that bedding on this limb continues in a ~80° SE dipping panel and nowhere forms a syncline required for separate folds. The parallel curvature of the bedding strike suggests the Atushi and Talanghe anticlines form over a common, linear structure and are not offset, linked anticlines (e.g. Sattarzadeh et al., 2000). We designate the entire anticline as the Atushi–Talanghe anticline, but refer to the Atushi and Talanghe anticlines to identify the western and eastern halves, respectively.

At transect A–A′, the Atushi anticline is isoclinal, dominated by an 80° dip panel on the southern limb and a 75° dip panel on the north (Fig. 8). The characteristic, dark Xiyu Formation conglomerate is clearly visible on the northern side but is absent on the southeast side (Fig. 2). Without the Atushi–Xiyu contact, the southern contact for the gravel was located by projecting beds in from ~4 km to the east. In the cross-section, the width of the fold was determined by the southernmost structural measurements and the requirement of no net structural relief between the synclines bounding the fold. The top of the anticline was modified to have a horizontal dip panel. This alteration contributes to a conservative shortening estimate, and is consistent with dip panels observed at the Boguzihe water gap and Mingyaole sections, and the gentle character of the anticlines at their tips.

At transect B–B′, the Boguzihe water gap (Fig. 9), the northernmost dip measurements for the 80° panel were measured ~1.7 km west of the profile on bedrock islands in an ephemeral channel. The southern limb contains an overturned panel that dips 87° to the north, which is connected to a steeply dipping panel (74°) by a long, gently dipping kink hinge visible in the lowest terrace riser. Where the Boguzihe enters New Atushi (Fig. 2), a remnant knob of sediments records the initiation of shortening in an abrupt set of reducing dips interpreted as syntectonic deposition (Chen et al., 2002). Paleomagnetic samples along this profile constrain the age of the strata (Figs. 2 and 4). Two fault scarps are located ~100 and ~400 m north of the core of the fold, offsetting several fluvial terraces of the Boguzihe. The geomorphic expression of the scarps in CORONA images indicates that the south dipping faults have been recently active. The location of these faults within the hinge zone of the anticline suggests that these faults accommodate deformation in the core, but are not causal thrusts of a fault propagation fold.

The southern limb of the Ganhangou traverse, located ~10 km west of the Boguzihe, has a uniform strike of N70E and a ~50° dip for 3 km that ends in off-lapping growth

Fig. 9. Cross-section interpretations for the Kashi–Atushi fold system. Bedding orientations and lithologic data were obtained by field mapping; (D) and (E) were improved with data from Chinese geologic maps (XBGM, 1965b) and (F) was constructed solely with the information from Chinese geologic maps (XBGM, 1965a). Conventions as in Fig. 8. The asterisk (*) identifies the beds used to calculate line length shortening. Transect C–C′ includes double detachment planes and low-angle, deep thrust faults interpreted from seismic reflection survey.

strata (Fig. 7). One of the magnetostratigraphic sections used in this paper was collected along this transect (Chen et al., 2002). A cross-section of this transect was not produced due to the erosion of the northern limb.

Transect C–C′, along the Seven Mills water gap, provides the most complete record of both limbs of the Talanghe anticline (Fig. 9). Similar to the Boguzi River section, the fold is tight, dominated by ~75° dipping limbs. The seismic reflection profile indicates that the total fold width is ~13 km, almost twice the size of its topographic expression (~7 km). Along the canyon walls, the hinge zone exhibits ~500 m of folded and disrupted bedding, bound on the southern side by a south dipping fault that is parallel to bedding in the hanging wall. Without stratigraphic marker beds, the offset on the fault is not quantifiable beyond the ~200 m offset provided by the exposure. Unique to this section, the seismic reflection profile contained two reverse faults and fault bends between depths of 9 and 12 km (Fig. 9). Beds translated across the 26°, south dipping fault ramp are offset by approximately 2 km.

In the northeast corner of the study area, the opposing tips of the Mutule and Talanghe anticlines fold the Xiyu Formation into an open syncline along transect D–D′ (Figs. 3 and 9). The blunt nose of the open Mutule anticline plunges more steeply than the tight Talanghe anticline. The Xiyu Formation is folded in the syncline to the east of the profile, and has been represented in the cross-section by locating the bottom of the contact just above the remaining topography along the transect. Growth strata were observed on the southern limb of the Talanghe anticline, but the northern limb of the Mutule anticline has been eroded.

3.2.2. Mingyaole anticline

The Mingyaole anticline is the smallest in the study area, ~40 km long and 10 km wide at the widest section. The fold has an arcuate shape and is impinged upon its southwest edge by the Kazikeaete thrust system and north verging Mushi anticline (Fig. 3). A fault associated with the Kazikeaete thrust ruptured in 1985 during the M 7.2 Wuqia earthquake, creating a 1.3 m dextral and ~1 m vertical offset (Chen et al., 1997; Molnar and Ghose, 2000). In cross-section, the Mingyaole anticline exhibits north vergence. Unlike the Atushi–Talanghe anticline, which expresses very tight folding at the surface, the Mingyaole anticline is broad. Also unique to the Mingyaole anticline, a series of unconformities we have interpreted to indicate the initiation of folding in this area were found below the base of the Xiyu Formation. Moving up section at the southern end of the Mingyaole transect, a >2 km thick, 58° dip panel ends as bedding dips abruptly decrease to 27°, and then are unconformably replaced by 13° dipping beds over a 50 m interval (Fig. 9). To produce this cross-section, the growth strata were modeled to deform progressively by limb rotation.

3.2.3. Kashi anticline

The axial trace of the Kashi anticline has an orientation similar to the Mingyaole anticline (N85E) but their tips are offset by ~5 km. The Kashi anticline is over 60 km long and is bisected by the Baishikeremuhe. As at the Talanghe anticline, deflected streams at the eastern end suggest the fold continues farther into the basin than indicated by its topographic expression or the Landsat image (Fig. 2). This interpretation is supported by a gentle fold exhibited in the seismic reflection profile that crossed ~15 km east of the topographic end of the fold. The width of the fold is constant across the fold, ~13 km at transects F–F′ and G–G′, but the fold amplitude is ~1.5 km lower at transect G–G′. Fanning strata are observed in the seismic profile on the north and south sides of the fold.

3.3. Calculated shortening

Slickenlines on bedding planes were observed throughout the study area, but were not considered pervasive. Similarly, small-scale accommodation features were scarce. We did not observe evidence of consistent deformation domains that suggest the folds formed by tangential longitudinal strain (e.g. neither tensile cracks in outer arcs nor reverse faults in deeper arcs). Due to the poorly indurated stratigraphy and vigorous erosion of the uplifted structure, we lack observational control on the internal character of the anticline, and thus on the mechanism(s) of shortening [e.g. homogeneous strain, second order faulting or second order folding (Epard and Groshong, 1995)]. The bulk of each limb, however, maintained broad, planar kink panels, and the limbs appear to control the largest scale morphology of the anticlines. We therefore present shortening estimates from two methods: excess area calculations and line length balancing (Table 1). Both methods assume that flexural slip is the dominant deformation mechanism.

3.3.1. Excess area

Flexural slip is accommodated by layer parallel shear, which can be displayed graphically in an apparent shortening plot (Fig. 10A; Mitra and Namson, 1989). All of the anticlines show a decrease in apparent shortening profile with depth, which suggests interbed shear increases in stratigraphically higher layers. In the case of disharmonic detachment folds, Mitra and Namson (1989) suggest the concentricity of the anticline is lost in the lower layers because space accommodation problems result in penetrative shortening, which changes the deformed bed length. In the Kashi–Atushi fold system, erosion limits our ability to evaluate macroscopic deformation in stratigraphically lower layers, so we assume that the differential penetrative shortening in lower layers balances the increase in interbed shear in higher layers.

Excess area, or the area encompassed by a fold under a particular stratigraphic level divided by the total shortening at that level, was first used by Chamberlin (1910) to

Table 1
Summary of shortening and shortening rate estimates for structural transects. The shortening estimates determined by excess area are considered more robust than the line length shortening

Transect	Excess area shortening (km) (preferred)	Line length shortening (km)	Shortening rate (mm/yr) using excess area shortening, assuming uniform initiation at 1.2 Ma	Slowest/fastest shortening rate[a] (mm/yr) using excess area shortening	Inferred initiation of folding[b] (Ma)	Shortening rate (mm/yr) assuming lateral propagation
Fig. 12 (H–H′)[c]	9.3	9.2	7.8	5.3/11.9	–	–
Atushi (A–A′)	6.8	5.5	5.7	3.8/8.7	2.0	3.4
Boguzihe (B–B′)	4.3	4.7	3.6	2.4/5.5	1.4	3.1
7 Mills (C–C′)	2.5	4.1	2.1	1.4/3.2	0.9	2.8
Mutule (D–D′)	2.4	1.8	2.0	1.4/3.1	0.8	3.0
Mingyaole (E–E′)	1.5	1.4	1.3	0.8/1.9	> 1.9	<0.8
Kashi Central (F–F′)	4.1	3.2	3.4	2.3/5.3	1.1	3.7
Kashi East (G–G′)	0.7	0.2	0.6	0.4/0.9	0.7	1.0

[a] Slowest rate calculated with fold initiation at 1.77 Ma, fastest rate calculated with fold initiation at 0.78 Ma. See text for explanation.
[b] Inferred from lateral propagation rate (50 km/Myr) defined between the Boguzihe and Ganhangou magnetostratigraphic sections (see Section 4).
[c] Includes line length shortening from the southern limb of the Keketamu anticline (4.3 km, Fig. 12).

Fig. 10. Results of (A) apparent shortening profile and (B) excess area method for each transect. From a maximum at the uppermost layer, the apparent shortening profiles reduce with depth, indicating a gradient in interbed shear. The true shortening profiles are unknown, because interbed shear can be balanced by penetrative deformation. (B) Excess area methods of Epard and Groshong (1993) calculate the shortening (the slope) and the depth to the detachment (the x intercept). Dashed lines show regression for the linear, upper part of the series, solid lines use all data from the transect.

determine the depth to the detachment horizon. For this study, we use the excess area method as adapted by Epard and Groshong (1993). This method compares the excess area at several stratigraphic levels with the depth from each level to a constant reference horizon (Fig. 10B). A plot of the relationship between the excess area and depth to the reference horizon gives the estimated shortening (the slope) and the depth to the detachment (the X-intercept). For this study, at least six excess areas were determined for each anticline and the land surface at each cross-section was plotted as the reference horizon. Shortening calculated by excess area varied from 6.8 km at Atushi to 0.7 km at the East Kashi transect (Table 1).

Excess area graphs of the Atushi, Boguzihe, Seven Mills, and Kashi cross-sections show a common feature, in that the slope (i.e. the shortening) is linear to a depth of 5.5–6.0 km below land surface at each profile (Fig. 10B). Above this depth, the slopes have a high correlation coefficient, suggesting that deformation mechanisms are balanced and bed lengths remain constant with deformation. Below this depth, the slope shallows, suggesting reduction in strain. This pattern is produced if the detachment horizon is raised over time, or if the detachment occurs over a zone with differential strain rather than a single detachment plane. Alternatively, the deformation gradient may change at lower depths, resulting in an imbalance between interbed shear and differential penetrative shortening. For this reason, two detachment horizons are considered. The upper detachment horizon is ~6 km below land surface, at the transition from constant bed lengths to imbalanced deformation mechanisms. Using all data, the maximum estimated depth to detachment is 8.6 km below land surface [due to very poor correlation ($R^2 = 0.6$) and an anomalously low depth to detachment estimate (13.4 km), the Kashi East transect is not included in the average]. We suggest that between 6 and 9 km, there is a reduction in north directed shortening and an increase in northward translation of material under the Tian Shan.

3.3.2. Line length balancing

For comparison with other regional estimates of shortening (Yin et al., 1998; Allen et al., 1999; Burchfiel et al., 1999), we also calculated line length changes for each profile (Table 1). This method assumes that the folding process does not alter the bedding from its original length. To capture the shortening of the youngest pregrowth deposits, the uppermost reconstructed bedding horizon was used (Figs. 8 and 9). With the exception of the Seven Mills and Kashi East transects, the correlation between the excess area and line length balancing methods is very good (±20%). Poor correlation at the Seven Mills transect probably results from the tightness of the fold. Poor correlation at the Kashi East transect may reflect the kinematics of the early stages of fold development (Poblet and McClay, 1996).

The shortening is linear for all transects to a depth of ~6 km below land surface, indicating interbed shear and penetrative deformation are balanced. Below ~6 km, the shortening is reduced, suggesting a gradient in folding down to the detachment plane, ~9 km below land surface.

4. Discussion

The style and form of these folds, as drawn, result from a set of interpretations concerning their deposition and geometry. Described in previous sections, the interpretation of the nature of the Xiyu–Atushi contact, conventions followed in reconstructing the anticlines, and the nature of the growth strata all affect the shortening estimates.

4.1. Structure

A basic assumption that influences the shortening estimates is the lack of structural height that developed across the folds Although the cross-sections were developed to minimize the height of the folds (principally by restricting the length of steeply dipping panels), not modeling the imbricate thrusts commonly required that the width of each fold was broadened from its surface expression by increasing the distance between the outer kink axes. The Kashi East transect (G–G′) is the only profile unaltered by this convention. The seismic lines, however, provide independent support for this modification, as they show that in the subsurface the folds are broader than their topographic expression, and lack clear evidence of thrust faults in the upper 6 km. Where seismic lines are available, the location of the outer kink axes in the cross-section interpretations does not contradict the seismic reflection data.

Interpretation of the Kashi–Atushi fold system as a set of detachment folds is supported by the strong competency contrasts in the deformed beds (Dahlstrom, 1990; Mitra, 2002). The Kashi Group contains a significant proportion of gypsiferous units, and shows severe small-scale folding and pervasive faulting where exposed in the southern Kepingtage system. The Wuqia Group is rich in siltstones, and shows a ductile behavior in areas of high strain, such as the core of the Boguzihe transect. The Atushi Formation exhibits second order faulting at the core of the Mingyaole, Atushi, and Boguzihe transects and second order folding at Seven Mills. In the limbs of each anticline, however, the Atushi Formation forms parallel-bedded kink panels with scarce to no faults. Finally, the Xiyu Formation appears to be the most competent, commonly forming the highest portions of the modern topography. Following the schema developed by Dahlstrom (1990), we interpret that the gypsiferous Kashi Group acts as a lower detachment plane, the upper Kashi and Wuqia Groups behave as a ductile detachment zone, and the Atushi and Xiyu Formations constitute a brittle upper layer that deforms by flexural slip

in the limbs and second order faulting and folding in the cores.

This mechanical stratigraphy permits limb rotation as a mechanism for fold growth (Dahlstrom, 1990), but the geometric similarity between these folds and symmetric faulted detachment folds suggests that limb lengthening also occurs (Mitra, 2002). Additional insight on the method of fold growth is provided by the anticlinal morphology. Detachment folding by limb rotation should be accompanied by a reduction in width and increased limb dips with advanced shortening. In contrast, shortening by limb lengthening should be accommodated by an increase in the height of the fold and a minor increase in fold width (Poblet and McClay, 1996). For each anticline, the fold widths remain fairly constant along strike, but the fold heights and limb dips are correlated with increased shortening (Figs. 8 and 9). This suggests that over the life of the folds, both mechanisms play a role in fold development. Unfortunately, the growth strata are insufficiently exposed to more precisely evaluate the kinematics of fold development (e.g. Salvini and Storti, 2002). In a future study, we hope to use deformed fluvial terrace surfaces to illuminate this question.

4.2. Paleomagnetic constraints

Magnetostratigraphic sampling across the Boguzihe and Ganhangou sections provides temporal constraints on the initiation of shortening (Figs 2 and 4; Chen et al., 2002) and allows an estimation of the shortening rate. The sections are linked together by tracing bedding along intervening strata and then matched to the geomagnetic polarity timescale (GPTS) of Cande and Kent (1995) constrained by the local Plio-Pleistocene fossil assemblage (Fig. 11). Sampling strategies and statistics, demagnetization processes, and correlation to the GPTS are described in detail in Chen et al. (2002). We apply their results to evaluate the initiation of shortening across the Kashi–Atushi fold system, and discuss implications for shortening rates.

The Boguzihe section is a good location to constrain the age of the base of the Xiyu Formation (~1.9 Ma), but the cobble conglomerate prevents paleomagnetic sampling through the syntectonic unconformity. Consequently, the age of the syntectonic unconformity at Boguzihe (~1.4 Ma) is calculated both from a linear extrapolation of the sedimentation rate of the underlying, dated strata and by strike line correlation to dated strata in the Ganhangou section (Fig. 11). At the Ganhangou section, finer grained sediments allow us to sample across the syntectonic unconformity and capture the age of the growth sediments. The age of the unconformity at Ganhangou (~1.2 Ma) is younger than at the Boguzihe section. Ages of the syntectonic unconformity are maxima; if some pregrowth strata are missing, the true age of the unconformity could be younger.

Upper and lower limits on the 1.2 Ma estimate for fold initiation are determined from the polarity sequence correlation to the GPTS (Fig. 11). Assuming both sites are correctly tied at the base of the Olduvai chron, the long reversed period containing the syntectonic unconformity at both sites cannot be older than the end of the Olduvai chron (1.77 Ma) and no younger than the beginning of the Bruhnes normal chron (0.78 Ma). Therefore, we choose upper and lower limits of 1.77 and 0.78 Ma, respectively, to bracket the initiation of folding. Records of small magnitude earthquakes (USGS Earthquake Hazards Program, 2003), geomorphic expression of fault scarps, (Zhao et al., 2000), warping of fluvial terrace surfaces, and geodetic studies (Wang et al., 2000) indicate that folding continues to the present.

4.3. Shortening rates

A simplistic approach to quantifying the geologic shortening rate is to identify a representative location and apply a regional initiation of folding at 1.2 Ma Expanding the region to a central profile (H–H′) including shortening accommodated in the southern limb of the Keketamu anticline (4.3 km) and the Boguzihe and Kashi East transects, the total shortening across the Kashi–Atushi fold system is 9.3 km (Fig. 12). If shortening across the three structures in this transect initiated contemporaneously, a mean shortening rate of 7.8 mm/yr has continued for the past 1.2 Myr (Fig. 13). Extreme minimum (5.3 mm/yr) and maximum (11.9 mm/yr) rates result from upper and lower age limits, respectively (Table 1). Shortening rates for each transect reduce to the east if folding was coeval (Table 1; Fig. 13).

While synchronous folding provides a reasonable estimate of the shortening rate, it is an unlikely condition because the stratigraphic height of the growth strata changes across the study area. At the Mingyaole profile, the growth strata are located just below the base of the Xiyu Formation whereas at the Boguzihe transect and the Ganhangou section, the growth strata are younger than the Xiyu Formation. To integrate these observations, we estimate the geologic shortening rate at each transect using the difference in growth strata ages at Boguzihe and Ganhangou (1.4 and 1.2 Ma, respectively). Dividing the distance between the sites (~10 km) by the difference in initiation of folding at Boguzihe and Ganhangou (0.2 Myr) results in an eastward lateral propagation rate of ~50 km/Ma. The eastern end of the Talanghe anticline shows geomorphic evidence of eastward lateral propagation (Fig. 14). However, the geomorphic expression of the anticline is 25 km shorter than expected if the lateral propagation rate has been constant for the last 1.2 Ma, suggesting that the extrapolated rate overestimates the true lateral propagation rate. If the propagation rate decreased to the east because stress was accommodated on the Mutule anticline, the lateral propagation rate can be used to estimate the initiation of folding across the Kashi–Atushi fold system, recognizing that

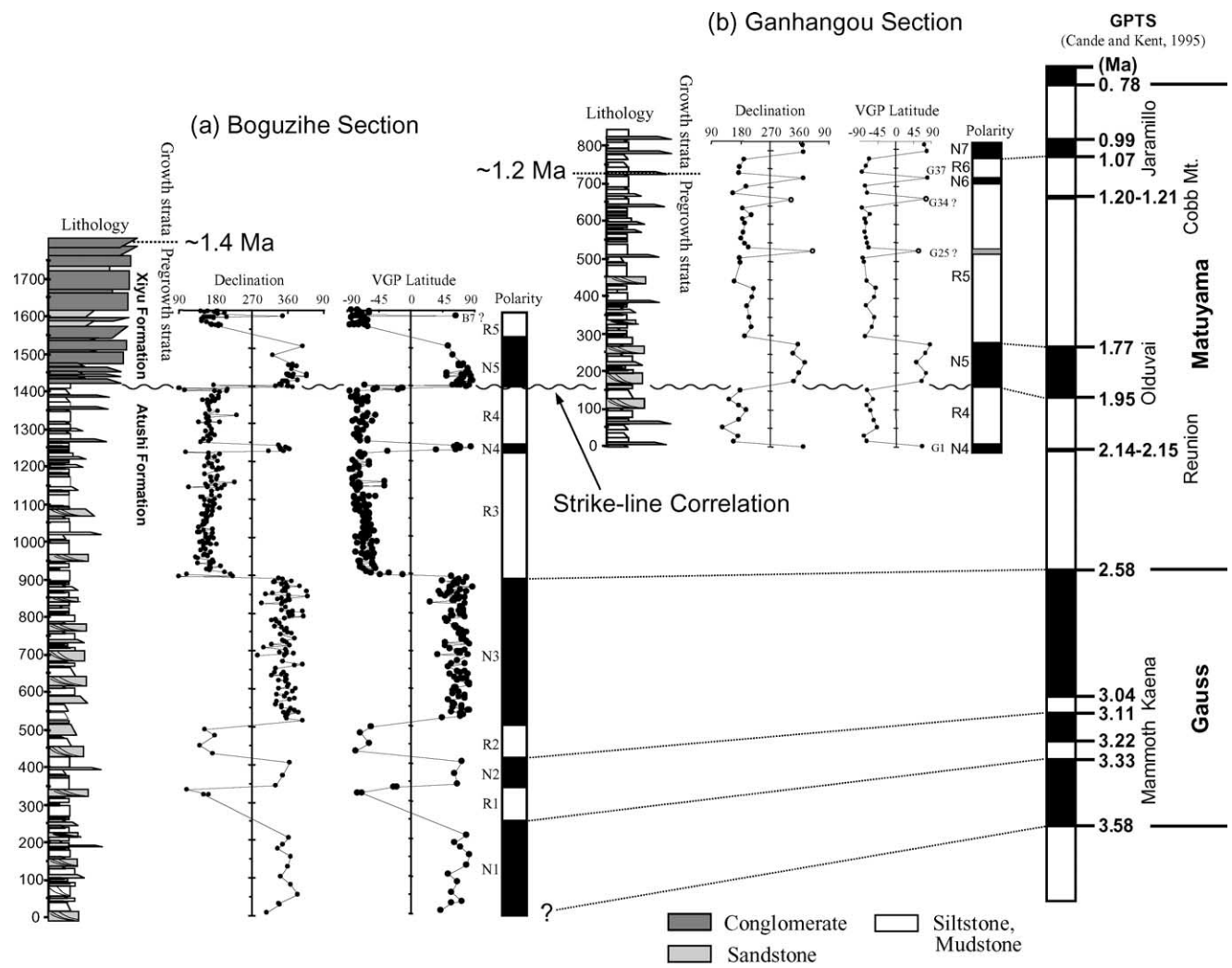

Fig. 11. Paleomagnetic results for the Boguzihe and Ganhangou sections compared with the GPTS (Cande and Kent, 1995). See Fig. 4 for location of the paleomagnetic sections. The sections were linked by tracing distinct beds ~10 km from the Boguzihe to the Ganhangou section (wavy line), and then correlated to the GPTS. The basal age of growth strata sampled at Ganhangou is inferred to be 1.2 Ma, whereas the age at Boguzihe (1.4 Ma) was calculated by extrapolating a constant sedimentation rate. At the Boguzihe section, the contact between the Xiyu and Atushi Formations is ~1.95 Ma. The Xiyu Formation is absent at the Ganhangou transect. Modified from Chen et al. (2002).

interpreting the sequence of fold development across the folds is speculative given vigorous erosion of the anticlines and uncertainty in the kinematics of fold growth.

To arrive at local estimates of the shortening rate, we simply extend the 50 km/Myr lateral propagation rate from the Ganhangou location back in time to the west and forward to the east (Table 1; Fig. 13). Under this assumption, the initiation of folding would occur ~2.0 Ma at the Atushi transect, ~0.9 Ma at the Seven Mills and ~0.8 Ma at the Mutule transect. Although considerably more speculative, we estimate the ages along the Mingyaole and Kashi anticlines using a similar technique and the same propagation rate. A seismic reflection profile ~20 km east of the topographic expression of the Kashi anticline shows low amplitude folding. If folding began at this end recently, the initiation of folding can be extrapolated westward from this location, assuming the Mingyaole and Kashi anticlines formed successively and deformation propagated eastward. From this construct, folding initiated at ~0.7 Ma at the East Kashi transect, ~1.1 Ma at the Central Kashi transect, and at least ~1.9 Ma at the Mingyaole transect (Table 1). Because the growth strata are older than the Xiyu Formation at Mingyaole, this scenario suggests that the Xiyu Formation at Mingyaole is younger than ~1.9 Ma, the same age as the base of the Xiyu at the Boguzihe transect (1.9 Ma). A western source for this conglomerate suggests the Pamir salient had reached this area by ~1.9 Ma, consistent with estimates for development of the Trans Alai Range around ~4 Ma (Arrowsmith and Strecker, 1999). While local shortening rates decrease to the east along the Atushi–Talanghe anticline, they are variable across the Mingyaole and Kashi anticlines. Restricted to the Kashi–Atushi fold system, we consider representative a regional average rate of ~5 mm/yr (Fig. 13).

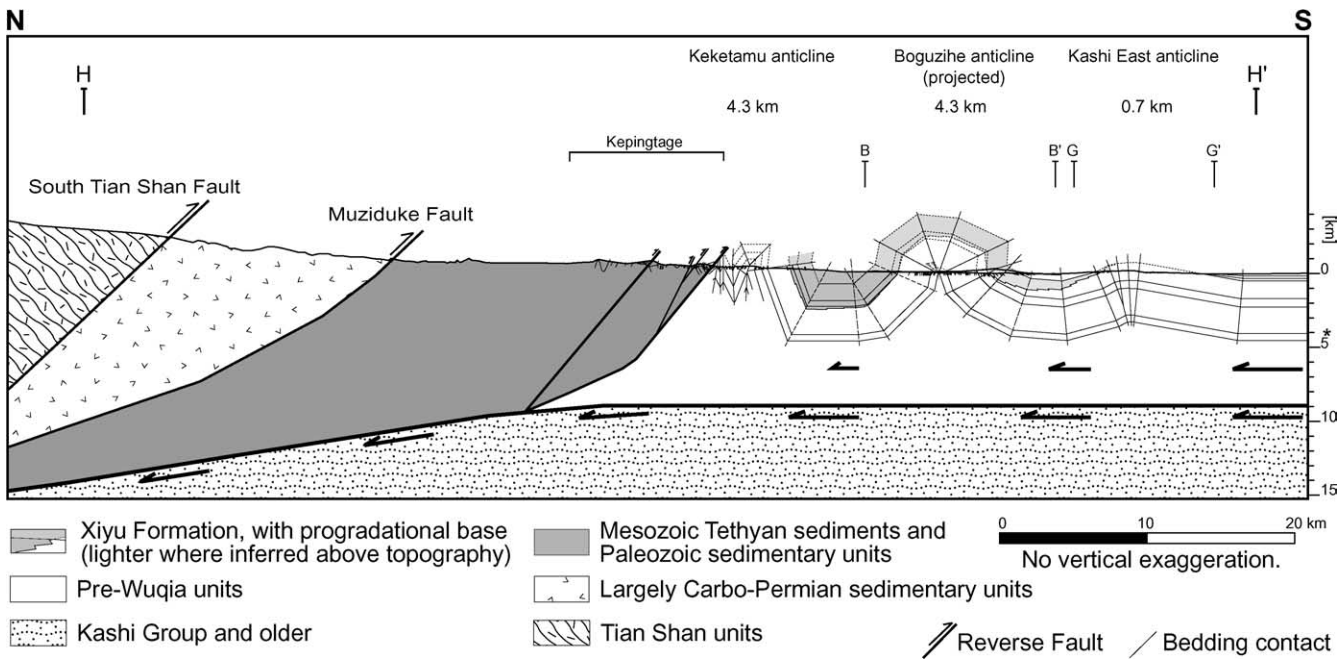

Fig. 12. Generalized cross-section across southern Tian Shan (H–H′ on Fig. 2). Total Pleistocene through modern shortening between the Keketamu and Kashi anticlines is 9.2 km. Due to uncertainties in the geometry of the northern margin of the Keketamu anticline, shortening accommodated by this structure was calculated by line length balancing. The bed used to measure the shortening is noted with an asterisk (*). Shortening calculated for the Boguzihe and Kashi East anticlines was determined by excess area methods. Arrows above detachment surface show decreasing slip to the north while the Tarim craton is underthrust below the Tian Shan. The fault geometry of the Kepingtage, South Tian Shan fault, and Muziduke fault, and the angle of the Tarim craton under the Tian Shan are not known and drawn schematically.

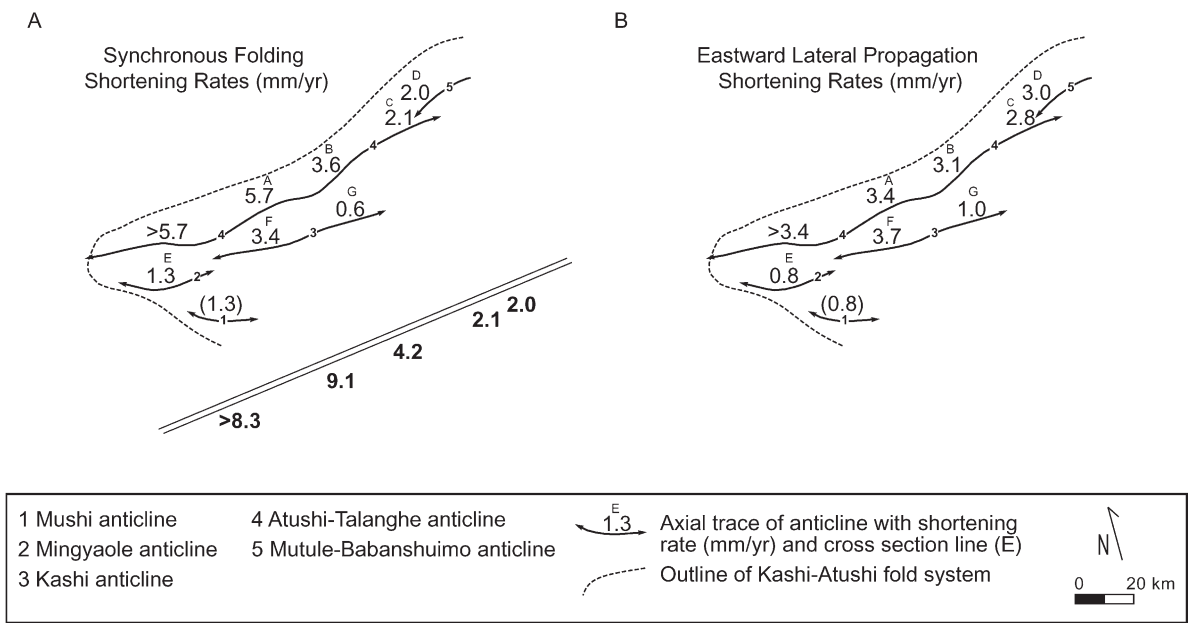

Fig. 13. Simplified maps of shortening rates determined along the Kashi–Atushi fold system assuming (A) uniform initiation (average rates for structure-perpendicular transects across the entire Kashi–Atushi fold system are presented under the double line) and (B) lateral propagation. We have not mapped the Mushi anticline, but its size and appearance suggest it has accommodated at least as much deformation as the Mingyaole anticline. These estimates are shown in parentheses, and added to the cross structure averages. (A) If folding was coeval, shortening rates reduce to the east by a factor of four. (B) If the folds grew laterally, the Atushi anticline formed first, followed by the Mushi and Mingyaole anticlines, then the Talanghe and Kashi anticlines.

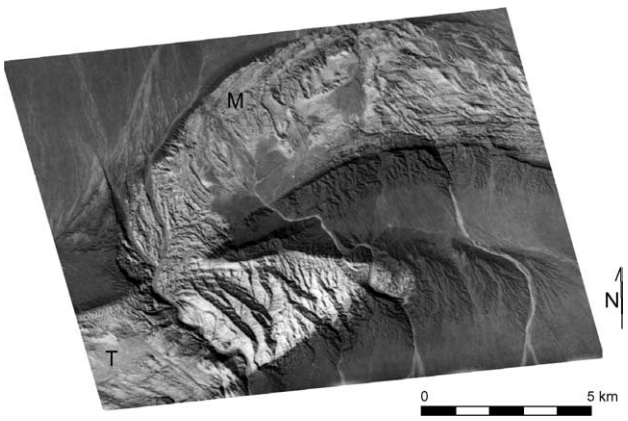

Fig. 14. CORONA satellite photo of confluence of Mutule (M) and Talanghe (T) anticlines. Light-colored rocks are Atushi Formation and darkest gray rocks are Xiyu Formation. Most of the folded Xiyu Formation in the syncline pre-dates the initiation of folding. The series of deflected drainages across the nose of the Talanghe anticline suggest its eastward propagation.

4.4. Regional kinematics

It is informative to compare timing and rate estimates presented here with those from other areas at the boundary between the Tarim Basin and the Tian Shan, beginning near Wenguri, just north of the study area, and proceeding clockwise around the Southern Tian Shan. Sobel and Dumitru (1997) sampled locations within the Kepingtage system for apatite fission track provenance and exhumation dates. They infer that thrusting north of Wenguri (Fig. 3) was active before 14 Ma and has propagated southward through time. This is consistent with our results and indicates that there was a ~12 Ma gap between initiation of activity on the Kepingtage system and the Kashi–Atushi fold system.

Allen et al. (1999) report on shortening to the east of the Kashi–Atushi fold system, along the Kepingtage thrust zone (Fig. 1). At that location, the shortening is expressed as thin-skinned, imbricate thrusts that have accommodated ~35 km of shortening within a ~100 km long zone. From the magnetostratigraphic results of Yin et al. (1998), they estimate that thrusting initiated around 20 Ma, resulting in an average shortening rate of ~1.8 mm/yr, if shortening spans the entire interval to the present. Farther east in the Kuche region (Fig. 1), magnetostratigraphic results by Yin et al. (1998) are used to date a lacustrine to fluvial transition inferred to represent regional thrust initiation, between 24 and 21 Ma. When applied to the 20–40 km of total shortening, the rate (1–1.9 mm/yr) is similar to the results in Kepingtage, but much lower than the rates at the Kashi–Atushi fold system.

Burchfiel et al. (1999) present cross-sections from both the northern and southern perimeters of the eastern Tian Shan (Fig. 1). These cross-sections show a structural style that is similar to our interpretation for the Kashi–Atushi fold system, and contrasts with imbricate thrusting observed along the Kepingtage and Kuche thrust systems. In particular, the Boston Tokar and Kalasu transects of Burchfiel et al. (1999) contain tight, upright folds and abrupt lithologic changes across the folds. Cross-sections on these transects yield shortening estimates of ~10–20 km, 1–4 times larger than estimated for the Kashi–Atushi fold system. To quantify the shortening rates, Burchfiel et al. (1999) used a range of initiation between 2.5 and 1.0 Ma (based on a climate inferred Quaternary age of a conglomerate), resulting in estimated shortening rates between 3 and 21 mm/yr.

Given uncertainty in the age of fold initiation at the Boston Tokar and Kalasu sections, the mean shortening rate (5.1 mm/yr) estimated for the Kashi–Atushi fold system is high compared with the more proximal Kepingtage and Kuche regions, and folding probably initiated more recently. This suggests that the setting of the Kashi–Atushi fold system may be unique. Indeed, it is located above the deepest depocenter in the Tarim Basin and shows little seismicity in comparison with the other systems.

We envision the Kashi–Atushi fold system as part of an accretionary wedge, formed as the Tarim craton is forced north and underthrust below the Tian Shan. Approximately 9 km of the Tarim craton has been underthrust below the Tian Shan in the last 1–3 Myr, which is resolved by the folding of the top 6 km of Cenozoic strata (Fig. 12). Structural evidence of parallel folding and geodetic evidence for northward directed shortening (Holt et al., 2000), combined with geophysical models of Bouger gravity anomalies (Burov et al., 1990) support this model. The two interpretations for initiation of shortening indicate that either the eastern end has been shortening more slowly or for less time (Fig. 13). In either case, the patterns of shortening rates may be facilitated by the Pamir Salient, which imposes a load on the westernmost Tarim Basin (Burov et al., 1990). In response to the load, the Tarim craton would be flexed more in the west, which potentially facilitates underthrusting of the western Tarim craton below the Tian Shan. In the eastern portion of the study area, the reduced effects of the load may inhibit underthrusting of the Tarim craton, and northward directed convergence would be taken up within the Tian Shan proper. The higher concentration of folds in the west may also be controlled by the geometry of the Kashi Depression, which was thickest in the west and thinned to the east.

5. Conclusions

The Kashi–Atushi fold system occupies a unique location in the Indian–Eurasia collision. The folds are located in an ~80° corner between the north verging frontal thrust of the Pamir (the Kazikeaete thrust system) and the Southern Tian Shan fault. We model the Atushi–Talanghe, Mutule, Mingyaole, and Kashi anticlines as detachment folds due to very steep limbs (60–90°), an absence of

emergent, fold bounding fault scarps or faults in proprietary seismic surveys. The results do not prescribe a kinematic history for the deformation, but limit the shortening estimates to the most constrained data, namely the dips of the beds and the stratigraphic depth of the syngrowth sediments.

Shortening estimates calculated from the cross-sections show that total shortening decreases towards the east and south; the Atushi anticline accommodated the most shortening (6.8 km), while the Talanghe anticline transects exhibit 4.3 and 2.5 km at the Boguzihe and Seven Mills water gaps, respectively. The transect crossing the eastern tip of the Talanghe anticline and the western end of the Mutule anticline yields a total shortening of 2.4 km. The southern set of folds generally accommodates less than the northern sets, with the Mingyaole anticline shortened by 1.5 km and the Kashi anticline by 4.1 km in the middle and 0.7 km at the east end. Shortening across the Talanghe anticline reduces to the east, suggesting that either (1) the folds are propagating eastward over time, or (2) shortening across the anticlines began everywhere at the same time, but the strain rate reduces to the east. In total, at least 6 km of the Tarim Craton has underplated the southern Tian Shan in the last 1–2 Myr.

The geometry of the folds, organized like a pleat in a folded fabric, proximity to the Pamir Mountains, and the north vergence of the system suggest that the fold system results from the expected convergence between the Tarim Basin and the Tian Shan, but is affected by northward movement of the Pamir Salient as well. The young and relatively fast deformation of the Kashi–Atushi fold system appears to be related to the abnormally thick Tertiary sediments in the Kashi foredeep and regional forces imparted by the Pamir Salient. Assuming coeval initiation, the shortening rates across the Kashi Atushi fold system reduce to the west, from ~9 to 2 mm/yr, with an average of ~5 mm/yr. If deformation at the Keketamu anticline is included, the shortening of rate (7.8 mm/yr) across the region plus the previously computed shortening rates in the Tian Shan (~13 mm/yr; Abdrakhmatov et al., 2002; Thompson et al., 2002) agrees with the geodetic rates of ~20–24 mm/yr (Abdrakhmatov et al., 1996; Holt et al., 2000) across the western Tian Shan.

Acknowledgements

This study was greatly improved by the detailed reviews of Mark Allen and Josep Poblet. Thanks also to Dennis Fletcher for GIS assistance and Richard Heermance for fieldwork. This research was supported by the Continental Dynamics program of the US NSF (EAR 9614765), and by the National Science Foundation of China grants 49834005 and 40372081.

References

Abdrakhmatov, K.Y., Aldazhanov, S.A., Hager, B.H., Hamburger, M.W., Herring, T.A., Kalabaev, K.B., Makarov, V.I., Molnar, P., Panasyuk, S.V., Prilepin, M.T., Reilinger, R.E., Sadybakasov, I.S., Souter, B.J., Trapeznikov, Y.A., Tsurkov, V.Y., Zubovich, A.V., 1996. Relatively recent construction of the Tien Shan inferred from GPS measurements of present-day crustal deformation rates. Nature 384(6608), 450–453.

Abdrakhmatov, K.Y., Weldon, R., Thompson, S., Burbank, D., Rubin, C., Miller, M., Molnar, P., 2002. Origin, direction, and rate of modern compression of the Central Tien Shan. Geology and Geophysics (Russian) 42(10), 1585–1609.

Al Saffar, M., 1993. Geometry of fault-propagation folds; method and application. Tectonophysics 223(3–4), 363–380.

Allen, M.B., Vincent, S.J., Wheeler, P.J., 1999. Late Cenozoic tectonics of the Kepingtage thrust zone: interactions of the Tien Shan and Tarim Basin, northwest China. Tectonics 18, 639–654.

Arrowsmith, J.R., Strecker, M.R., 1999. Seismotectonic range-front segmentation and mountain-belt growth in the Pamir–Alai region. Kyrgyzstan (India–Eurasia collision zone). Geological Society of America Bulletin 111(11), 1665–1683.

Avouac, J.-P., Tapponnier, P., Bai, M., You, H., Wang, G., 1993. Active thrusting and folding along the northern Tien Shan and late Cenozoic rotation of the Tarim relative to Dzungaria and Kazakhstan. Journal of Geophysical Research 98(4), 6755–6804.

Bally, A.W., Chou, I.-M, Clayton, R., Engster, H.P., Kidwell, S., Meckel, L.D., Ryder, R.T., Watts, A.B., Wilson, A.A., 1986. Notes on sedimentary basins in China; report of the American Sedimentary Basins Delegation to the People's Republic of China. U.S. Geological Survey Open-File Report 86-327, pp. 93–95.

Bullen, M.E., Burbank, D.W., Abdrakhmatov, K.Y., Garver, J., 2001. Late Cenozoic tectonic evolution of the northwestern Tien Shan: constraints from magnetostratigraphy, detrital fission track, and basin analysis. Geological Society of America Bulletin 113, 1544–1559.

Burbank, D.W., McLean, J.K., Bullen, M., Abdrakhmatov, K.Y., Miller, M.M., 1999. Partitioning of intermontane basins by thrust-related folding, Tien Shan, Kyrgyzstan. Basin Research 11(1), 75–92.

Burchfiel, B.C., Brown, E.T., Qidong, D., Xianyue, F., Jun, L., Molnar, P., Jianbang, S., Zhangming, W., Huichuan, Y., 1999. Crustal shortening on the margins of the Tien Shan, Xinjiang, China. International Geology Review 41(8), 665–700.

Burov, E.B., Kogan, M.G., Lyon-Caen, H., Molnar, P., 1990. Gravity anomalies, the deep structure, and dynamic processes beneath the Tien Shan. Earth and Planetary Science Letters 96, 367–383.

Burtman, V.S., Molnar, P., 1993. Geological and geophysical evidence for deep subduction of the continental crust beneath the Pamir. Geological Society of America Special Paper 281, 76.

Burtman, V.S., Skobelev, S.F., Molnar, P., 1996. Late Cenozoic slip on the Talas–Ferghana fault, the Tien Shan, central Asia. Geological Society of America Bulletin 108(8), 1004–1021.

Cande, S.C., Kent, D.V., 1995. Revised calibration of the geomagnetic polarity timescale for the Late Cretaceous and Cenozoic. Journal of Geophysical Research 100, 6093–6095.

Carroll, A.R., Graham, S.A., Hendrix, M.S., Ying, D., Zhou, D., 1995. Late Paleozoic tectonic amalgamation of northwestern China; sedimentary record of the northern Tarim, northwestern Turpan, and southern Junggar basins. Geological Society of America Bulletin 107(5), 571–594.

Chamberlin, R.T., 1910. The Appalachian folds of central Pennsylvania. Journal of Geology, 228–251.

Chen, J., Qu, G., Feng, X., Hu, J., 1997. Arcuate thrust tectonics and its contemporary seismicity in the eastern section of the external zone of the Pamir. Seismology and Geology (Chinese with English abstract) 19(4), 301–312.

Chen, J., Ding, G.Y., Burbank, D.W., Scharer, K.M., Rubin, C., Sobel, E., Qu, G., Shen, J., Yin, J., Zhao, R., 2001. Late Cenozoic tectonics and

seismicity in the Southwestern Tian Shan, China. Earthquake Research in China (Chinese with English abstract) 17(2), 134–155.

Chen, J., Burbank, D.W., Scharer, K.M., Sobel, E., Yin, J., Rubin, C., Zhao, R., 2002. Magnetochronology of the upper Cenozoic strata in the southwestern Chinese Tian Shan; rates of Pleistocene folding and thrusting. Earth and Planetary Science Letters 195(1–2), 113–130.

Dahlstrom, C.D., 1990. Geometric constraints derived from the law of conservation of volume and applied to evolutionary models for detachment folding. American Association of Petroleum Geologists Bulletin 74(3), 336–344.

Epard, J.L., Groshong, R.H., 1993. Excess area and depth to detachment. American Association of Petroleum Geologists Bulletin 77, 1291–1302.

Epard, J.L., Groshong, R.H., 1995. Kinematic model of detachment folding including limb rotation, fixed hinges and layer-parallel strain. Tectonophysics 245, 85–103.

Harvard CMT, 2003. Centroid-Moment Tensor Project. http://www.seismology.harvard.edu/CMTsearch.html.

Hendrix, M.S., Graham, S.A., Carroll, A.R., Sobel, E.R., McKnight, C.L., Schulein, B.J., Zuoxun, W., 1992. Sedimentary record and climatic implications of recurrent deformation in the Tian Shan; evidence from Mesozoic strata of the north Tarim, south Junggar, and Turpan basins, Northwest China. Geological Society of America Bulletin 104(1), 53–79.

Holt, W.E., Chamot-Rooke, N., Le Pichon, X., Haines, A.J., Shen-Tu, B., Ren, J., 2000. Velocity field in Asia inferred from Quaternary fault slip rates and Global Positioning System observations. Journal of Geophysical Research 105(8), 19,185–19,209.

Hu, B., 1992. Petroleum geology and prospects of the Tarim (Talimu) Basin, China. In: Halbouty, M.T., (Ed.), Giant Oil and Gas Fields of the Decade 1978–1988, AAPG Memoir, 54, pp. 493–510.

Hu, L.Y., 1982. Late Tertiary foraminifera of Tarim Basin and their geological significance. Chinese Science Bulletin 15, 938–941.

Jamison, W.R., 1989. Fault–fracture strain in Windgate Sandstone. Journal of Structural Geology 11, 959–974.

Mao, S., Norris, G., 1988. Late Cretaceous–early Tertiary dinoflagellates and acritarchs from the Kashi area, Tarim Basin, Xinjiang Province, China. Life Science Contributions, Royal Ontario Museum 150, 93.

Marshak, S., Mitra, G., 1988. Basic Methods of Structural Geology, Prentice Hall, Englewood Cliffs, pp. 277–281.

Mitra, S., 2002. Structural models of faulted detachment folds. Association of Americal Petroleum Geologists Bulletin 86(9), 1673–1694.

Mitra, S., Namson, J.S., 1989. Equal-area balancing. American Journal of Science 289(5), 563–599.

Molnar, P., Ghose, S., 2000. Seismic movements of major earthquakes and the rate of shortening across the Tien Shan. Geophysical Research Letters 27(16), 2377–2380.

Molnar, P., Tapponnier, P., 1975. Cenozoic tectonics of Asia: effects of a continental collision. Science 189(4201), 419–426.

Neil, E.A., Houseman, G.A., 1997. Geodynamics of the Tarim Basin and the Tian Shan in Central Asia. Tectonics 16(4), 571–584.

Poblet, J., McClay, K., 1996. Geometry and kinematics of single-layer detachment folds. American Association of Petroleum Geologists Bulletin 80, 1085–1109.

Poblet, J., McClay, K., Storti, F., Munoz, J.A., 1997. Geometries of syntectonic sediments associated with single-layer detachment folds. Journal of Structural Geology 19(3–4), 369–381.

Rubin, C.M., Chen, J., Burbank, D., Scharer, K.M., Zhao, R., 2000. Late Cenozoic deformation along the western Kashi–Aksu thrust belt, Southern Tien Shan, China. Geological Society of America Abstracts with Programs 32, 1.

Salvini, F., Storti, F., 2002. Three-dimensional architecture of growth strata associated to fault-bend, fault-propagation, and decollement anticlines in non-erosional environments. Sedimentary Geology 146(1–2), 57–73.

Sattarzadeh, Y., Cosgrove, J.W., Vita-Finzi, C., 2000. The interplay of faulting and folding during the evolution of the Zagros deformation belt. In: Cosgrove, J.W., Ameen, M.S. (Eds.), Forced Folds and Fractures, Geological Society Special Publications, 169., pp. 187–196.

Scharer, K.M., Chen, J., Burbank, D., Rubin, C.M., Zhao, R., 2000. Quaternary folding of foreland basin strata at the boundary between the Northwest Tarim Basin and the Southern Tien Shan, China. Geological Society of America Abstracts with Programs 32, 1.

Sobel, E.R., 1999. Basin analysis of the Jurassic–Lower Cretaceous southwest Tarim Basin, northwest China. Geological Society of America Bulletin 111, 709–724.

Sobel, E.R., Dumitru, T.A., 1997. Thrusting and exhumation around the margins of the Western Tarim Basin during the India–Asia collision. Journal of Geophysical Research 102, 5043–5063.

Sobel, E., Mikolaichuk, A., Chen, J., Burbank, D., 2000. Development of the Late Cenozoic Central Tian Shan in Kyrgyzstan and China Recorded by Apatite Fission Track Thermochronology. Eos Transactions, AGU 91, 48, Fall Meeting Supplement, Abstract T71D-03.

Suppe, J., Medwedeff, D.A., 1990. Geometry and kinematics of fault-propagation folding. Eclogae Geologicae Helvetiae 83(3), 409–454.

Thompson, S., Weldon, R.J., Rubin, C.M., Abdrakhmatov, K., Molnar, P., Berger, G.W., 2002. Late Quaternary slip rates across the central Tien Shan, Kyrgyz Republic, central Asia. Journal of Geophysical Research 107(9), 20020910.

USGS Earthquake Hazards Program, 2003. http://neic.usgs.gov/neis/bulletin/03_EVENTS/eq_030224/neic_qqac_h.html.

Wang, Q., Ding, G., Qiao, X., Wang, X., 2000. Research on present crustal deformation in the southern Tian Shan (Jiashi) region by GPS geodesy. Acta Seismologica Sinica (English version) 13(3), 280–287.

Watson, M.P., Hayward, A.B., Parkinson, D.N., Zhang, Z.M., 1987. Plate tectonic history, basin development and petroleum source rock deposition onshore China. Marine and Petroleum Geology 4, 205–225.

XBGM, 1965. Xinjiang Bureau of Geology and Mineral Resources. Geologic Map of Kashi Anticline, scale 1:50,000.

XBGM, 1965. Xinjiang Bureau of Geology and Mineral Resources. Geologic Map of Mingyaole Anticline, scale 1:50,000.

XBGM, 1985. Xinjiang Bureau of Geology and Mineral Resources. Geological Map of southwestern Xinjiang. Geological Publishing, Beijing, scale 1:500,000.

Yang, H., 1996. Tertiary. In: Zhou, Z., Dean, W.T. (Eds.), Phanerozoic Geology of Northwest China, pp. 274–278.

Yin, A., Nie, S., 1996. Phanerozoic palinspastic reconstruction of China and its neighboring regions. In: Yin, A., Harrison, M. (Eds.), Tectonic Evolution of Asia, pp. 442–485.

Yin, A., Nie, S., Craig, P., Harrison, T.M., Ryerson, F.J., Xianglin, Q., Geng, Y., 1998. Late Cenozoic tectonic evolution of the southern Chinese Tien Shan. Tectonics 17(1), 1–27.

Zhang, P., Molnar, P., Downs, W.R., 2001. Increased sedimentation rates and grain sizes 2–4 Myr ago due to the influence of climate change on erosion rates. Nature 410, 891–897.

Zhao, R., Jun, L., Jun, S., 2000. The preliminary study on active faults and paleo-earthquakes in the north fringe of Kashi Depression. Acta Seismologica Sinica (English version) 13(3), 351–355.

Zhou, Z.Y., Chen, P.J., 1990. Biostratigraphy and Geologic Evolution: Petroleum Geology of Tarim Basin, Science Press, Beijing, China, 439pp.